

EXTENDED OBJECT TRACKING USING HIERARCHICAL TRUNCATION MODEL WITH PARTIAL-VIEW MEASUREMENTS

Yuxuan Xia*, Pu Wang, Karl Berntorp, Hassan Mansour, Petros Boufounos, and Philip V. Orlik

Mitsubishi Electric Research Laboratories (MERL), Cambridge, MA 02139, USA

ABSTRACT

This paper introduces the hierarchical truncated Gaussian model in representing automotive radar measurements for extended object tracking. The model aims at a flexible spatial distribution with adaptive truncation bounds to account for partial-view measurements caused by self-occlusion. Built on a random matrix approach, we propose a new state update step together with an adaptively update of the truncation bounds. This is achieved by introducing spatial-domain pseudo measurements and by aggregating partial-view measurements over consecutive time-domain scans. The effectiveness of the proposed algorithm is verified on a synthetic dataset and an independent dataset generated using the MathWorks Automated Driving toolbox.

Index Terms— Automotive radar, Bayesian filtering, object tracking, extended object, random matrix, autonomous driving.

1. INTRODUCTION

Autonomous driving has been in the spotlight over the past decade. Along with ultrasonic, camera and LIDAR sensors, automotive radar assists reliable environmental perception in all-weather conditions with affordable costs. This paper focuses on object tracking using automotive radar measurements. Within this context, extended object tracking (EOT), i.e., the tracking of an object that may give rise to one measurement per time scan, can lead to improved tracking capability over conventional point object tracking by augmenting the object state to both kinematic and extent states. A recent overview of EOT literature can be found in [1].

A measurement model is required to enable a Bayesian filtering framework for EOT. This likelihood needs to capture not only the spatial model, i.e., how radar measurements are spatially distributed around the object, but also characteristics of sensor noise. Early efforts include a model of a fixed set of points on a rigid body that requires a non-scalable data association between the fixed set of points and radar measurements [2–4]. Flexible spatial models have gained more attention. In these approaches, automotive radar measurements are spatially distributed as a function of individual measurement likelihoods, also referred to as the spatial distribution.

For automotive radar measurements, the spatial distribution can be generally divided into three categories: 1) contour models that reflect the measurement distribution along the contour [5]; 2) surface models that assume the radar measurements are generated from the inner surface of objects [6, 7]; and 3) surface-volume models that balance between the above models with more realistic features. For the contour model, typical examples include a rectangular shape model around four edges in [8, 9] and curve approximations using either Gaussian processes in [10, 11] or B-Spline model in [12].

*Y. Xia is a PhD student at Chalmers University of Technology, Sweden. This work was done during his internship at MERL.

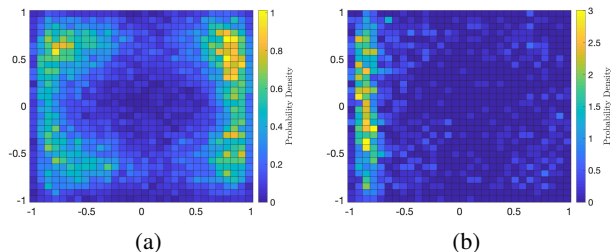


Fig. 1: Aggregated real-world automotive radar measurements (nuScenes dataset [17]) in a normalized object coordinate system. (a): full-view; and (b) partial-view with relative sensor aspect angle in the range $(-\pi/8, \pi/8)$.

For the surface model, a widely used model is the random matrix approach [6, 13–16] where objects are assumed to have elliptical shapes. The surface model often leads to computationally simpler algorithms than the contour model, which requires more degrees of freedom to describe more complex shapes.

As shown in Fig. 1, real-world automotive radar measurements rarely follow the above two types of spatial distributions. Two observations from Fig. 1 can be made: 1) measurement likelihoods are significantly lower at the center than those in a vicinity around outer edges; and 2) measurements exhibit self-occlusion features: measurement likelihoods are dominant at object parts that are closed to the automotive radar sensor. The first observation has motivated recent developments of surface-volume models including a volcanormal measurement model [18] and a completely data-driven measurement model by training real-world automotive radar measurements using a variational Gaussian mixture [19]. In comparison, there are few attempts to consider the second observation.

In this paper, we introduce a flexible measurement model to resemble the real-world spatial distribution of automotive radar measurements on vehicles with self-occlusion, thereby solving the two issues arisen in the above observations simultaneously. This is achieved by introducing a hierarchical truncated Gaussian measurement model with, possibly adaptive, truncation bounds. Specifically, the hierarchical model introduces a latent variable to denote noise-free measurement sources and to enforce the measurement feature that radar measurements are more likely to appear around object edges with a certain volume, while the noise is added to the measurement sources to model the observable measurements. The self-occlusion feature is accounted for by treating the truncation bounds as deterministic but unknown model parameters. To integrate the proposed measurement model into the Bayesian filtering framework, we develop a modified measurement update step within the random matrix model of [13] with the introduction of spatial-domain pseudo measurements and time-domain scan aggregation. Moreover, we introduce an online estimation step to adaptively update the truncation bounds for a more accurate spatial distribution.

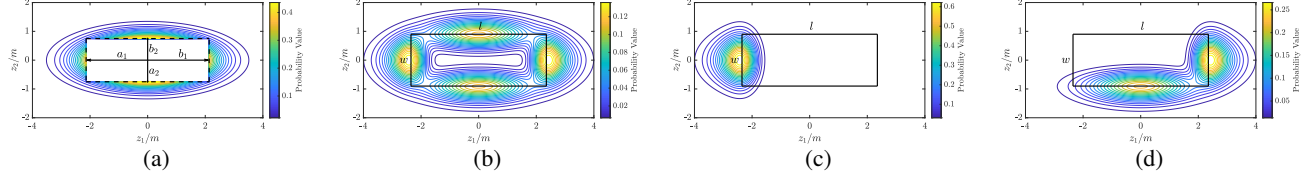


Fig. 2: (a): Probability density of the measurement source $p(y_k^j|\xi_k)$ centered at the origin of coordinates with $\rho = 0.25$, $l = 4.7$, $w = 1.8$, $a_1 = b_1 = 2.14$ and $a_2 = b_2 = 0.75$; (b): spatial distribution $p(z_k^j|\xi_k)$ with $R_k = \text{diag}([0.09, 0.09])$; (c) spatial distribution $p(z_k^j|\xi_k)$ with $a_1 = 2.14$ and $a_2 = b_1 = b_2 = \infty$; (d) spatial distribution $p(z_k^j|\xi_k)$ with $a_2 = 2.14$, $b_1 = 0.75$ and $a_1 = b_2 = \infty$.

2. PROBLEM FORMULATION AND SIGNAL MODEL

We define the object state as a tuple $\xi_k = (x_k, X_k)$ with $x_k \in \mathbb{R}^{d_x}$ denoting the *kinematic* state and $X_k \in \mathbb{S}_{++}^2$, a symmetric and positive definite matrix, denoting the *extent* state. The object length l and width w can be extracted from the normalized eigen-decomposition of X_k . For each time step k , we receive n_k measurements $Z_k \triangleq \{z_k^j\}_{j=1}^{n_k}$ from automotive radar sensors. The objective of object tracking is to recursively compute the posterior density of the object state $p(\xi_k|Z_{1:k})$ given all measurements $Z_{1:k} = \{Z_1, \dots, Z_k\}$ up to and including time k . The object state ξ_k with corresponding uncertainty measures can then be extracted from the posterior density $p(\xi_k|Z_{1:k})$.

Given the posterior density $p(\xi_{k-1}|Z_{1:k-1})$ at time $k-1$ and the transition density $p(\xi_k|\xi_{k-1})$, the predicted density can be obtained from the Chapman-Kolmogorov equation

$$p(\xi_k|Z_{1:k-1}) = \int p(\xi_{k-1}|Z_{1:k-1})p(\xi_k|\xi_{k-1})d\xi_{k-1}. \quad (1)$$

Given the predicted density and the current measurements Z_k , the posterior density at time k can be obtained using the Bayes update

$$p(\xi_k|Z_{1:k}) \propto p(\xi_k|Z_{1:k-1})p(Z_k|\xi_k), \quad (2)$$

where $p(Z_k|\xi_k) = \prod_{j=1}^{n_k} p(z_k^j|\xi_k)$ is the joint measurement likelihood with $p(z_k^j|\xi_k)$ denoting the spatial distribution. We approximate the predicted and posterior state densities such that they are all of the same functional form, which allows a recursive use of the prediction and update functions.

We model each measurement z_k^j as $z_k^j = y_k^j + v_k^j$, where v_k^j denotes the Gaussian distributed sensor noise $\mathcal{N}(v_k^j; 0, R_k)$ with diagonal measurement noise covariance R_k . The distribution of the hidden *measurement source* y_k^j , conditioned on the object state, is modeled as a truncated Gaussian

$$\mathcal{T}\mathcal{N}(y_k^j; Hx_k, \rho X_k, D_k) = \frac{\mathbf{1}_{D_k}(y_k^j)}{c_{D_k}} \mathcal{N}(y_k^j; Hx_k, \rho X_k), \quad (3)$$

where H is the observation matrix, ρ is a scaling factor, D_k specifies the truncated Gaussian density support, $\mathbf{1}_{D_k}(\cdot)$ is the indicator function on D_k , and c_{D_k} is the corresponding normalization factor. The truncated area is described by $B_k \triangleq [a_{k,1}, a_{k,2}, b_{k,1}, b_{k,2}]^T \geq 0$ with respect to the object center Hx_k and it is assumed that the orientation of the truncated area is the same as that of the object; see Fig. 2 (a) for an illustration. It is met that $B_k \uplus D_k = \mathbb{R}^2$.

Given the hierarchical measurement model above, the resulting spatial distribution $p(z_k^j|\xi_k)$ can be computed by marginalizing out the measurement source y_k^j , yielding

$$\begin{aligned} p(z_k^j|\xi_k) &= \int p(z_k^j|y_k^j)p(y_k^j|\xi_k)dy_k^j \\ &= \frac{1}{c_{D_k}} \int_{D_k} \mathcal{N}(z_k^j; y_k^j, R_k) \mathcal{N}(y_k^j; Hx_k, \rho X_k) dy_k^j. \end{aligned} \quad (4)$$

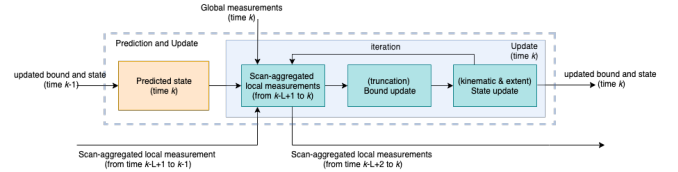


Fig. 3: Proposed partial-view EOT algorithm with scan-aggregation and on-line bound update.

One example of such marginalized measurement likelihood is shown in Fig. 2 (b). It can be seen that the hierarchical truncation model pushes the measurement likelihood away from the object center onto four edges, reasonably resembling the distribution of real-world automotive radar measurements, c.f. Fig. 1 (a).

To enable the modelling of partial-view measurements, the proposed measurement model allows one or more bound parameters of B_k to be infinity. For instance, when the object is observed from the behind, one can set $a_2 = b_1 = b_2 = \infty$ with adaptively estimated a_1 to concentrate the spatial distribution around the rear part; see Fig. 2 (c). Similarly, one can set $a_1 = b_2 = \infty$ with estimated a_2 and b_1 when the object is measured from the front right side; see Fig. 2 (d).

3. PROPOSED EOT ALGORITHM

In the following, we introduce the prediction and update steps of the proposed EOT algorithm, as shown in Fig. 3. We assume that both the predicted and posterior state densities have the factorized form [13]

$$\begin{aligned} p(\xi_k|Z_{1:k'}) &\approx p(x_k|Z_{1:k'})p(X_k|Z_{1:k'}) \\ &= \mathcal{N}(x_k; m_{k|k'}, P_{k|k'})\mathcal{IW}(X_k; \nu_{k|k'}, V_{k|k'}), \end{aligned} \quad (5)$$

where $k' = k-1$ is for the state prediction and $k' = k$ for the state update. The kinematic state x_k is Gaussian distributed with predicted/posterior mean $m_{k|k'}$ and covariance matrix $P_{k|k'}$, whereas the extent matrix X_k is inverse Wishart distributed with $\nu_{k|k'}$ degrees of freedom and the scale matrix $V_{k|k'}$.

3.1. Prediction step

We assume that the state transition density is approximated as a product of Gaussian and Wishart distributions [6]. Given the state transition density [20, Eq. (6)] and the posterior density $p(\xi_{k-1}|Z_{1:k-1})$ in (5), the predicted parameters $\{m, P, \nu, V\}_{k|k-1}$ can be (approximately) calculated as [13]

$$m_{k|k-1} = g(m_{k-1|k-1}), \quad G_{k-1} = \nabla_x g(x)|_{x=m_{k-1|k-1}}, \quad (6)$$

$$P_{k|k-1} = G_{k-1}P_{k-1|k-1}G_{k-1}^T + Q_{k-1}, \quad (7)$$

$$\nu_{k|k-1} = 6 + e^{-T_s/\tau}(\nu_{k-1|k-1} - 6), \quad (8)$$

$$V_{k|k-1} = e^{-T_s/\tau} E_{m_{k-1}} V_{k-1|k-1} E_{m_{k-1}}^T, \quad (9)$$

where T_s is the sampling time, τ is a maneuvering correlation constant, $g(\cdot)$ denotes a kinematic state motion model, Q denotes the process noise covariance and E denotes the transformation matrix, typically a rotation matrix depending on x .

3.2. Update Step

As shown in Fig. 3, the state update runs iteratively over three building blocks: 1) scan-aggregated measurements in a sliding window with length L , 2) truncation bounds update, and 3) kinematic and extent states update, until a convergence criteria is met. At the t -th iteration, we first convert the measurements at the latest time scan k into local measurements in the object coordinate system (OC) using the updated state estimates $\xi_{k|k}^{(t-1)}$ from the $(t-1)$ -th iteration. With the scan-aggregated local measurements from time step $k-L+1$ to the latest time step k , the truncation bounds specified by $B_k^{(t)}$ are updated using the maximum likelihood (ML) estimation. With the updated bounds and the new measurements at time step k , the kinematic and extent states are updated using a modified random matrix approach. At the first iteration, i.e., $t=0$, we may replace $\xi_{k|k}^{(0)}$ with the predicted state estimate $\xi_{k|k-1}$ to initialize the algorithm.

3.2.1. Filtered Scan-Aggregated Measurements

To obtain accurate estimate of the truncation bounds, we can make use of the filtered scan-aggregated measurements from past time scans to update the truncation bounds¹; see Fig. 4 for an illustration. This aggregation can be useful when the automotive radar measurements are sparse and partial-viewed due to self-occlusion. Given a measurement z in the global coordinate system (GC) and the mean m of the object kinematic state, the corresponding measurement in the OC at the t -th iteration can be obtained as

$$z_{OC}^{(t)} = M_m^{-1} (z - Hm^{(t-1)}), \quad (10)$$

where M_m is a rotation matrix that can be constructed using the object kinematic mean $m^{(t-1)}$. And $Z_{OC}^{(t)}$ groups all local measurements at the t -th iteration.

At the last T -th iteration, the corresponding local measurements are saved for scan aggregation. Specifically, we have

$$z_{OC,k}^j = z_{OC}^{(T+1)} = M_m^{-1} (z_k^j - Hm^{(T-1)}), \quad (11)$$

and $Z_{OC}^k = \{z_{OC,k}^j\}_{j=1}^{n_k}$ denotes the filtered scan-aggregated measurements from time step k . With a sliding window size L , the filtered scan-aggregated measurement set is denoted as $Z_{OC}^{k-L+1:k} = \{Z_{OC}^{k-L+1}, \dots, Z_{OC}^k\}$.

3.2.2. Adaptive Update of Truncation Bounds

By grouping the filtered scan-aggregated measurements $Z_{OC}^{k-L+1:k}$ and the new local measurement $Z_{OC}^{(t)}$ into $Z_{OC}^{(t),k-L+1:k}$, the truncation bounds are updated as follows. The ML estimate $\hat{B}_k^{(t)}$ of the truncation bounds at the t -th iteration is given by

$$\arg \min_{B_k^{(t)}} \sum_{z \in Z_{OC}^{(t),k-L+1:k}} -\log p(z|\xi_k^{(t-1)}, B_k^{(t)}), \quad (12)$$

¹When the measurements are very sparse, there might not be enough information to give an accurate estimate of the truncation bounds.

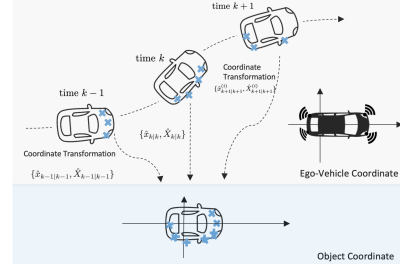


Fig. 4: Filtered scan aggregation in object coordinate (OC) system.

where $p(z|\xi_k^{(t-1)}, B_k^{(t)})$ is of the form of (4) that involves both the normalization factor c_{D_k} and the truncated area $D_k = \mathbb{R}^2 \setminus B_k^{(t)}$. The ML estimation of the four truncation bounds needs to compute the integration over D_k and directly solving (12) can be computationally demanding for online update.

To address this issue, we propose to divide the scan-aggregated measurements into four clusters using the expectation-maximization algorithm [21], which effectively decomposes the joint ML bound update into up to four decoupled ML estimates of the truncation bound. We now explain the procedure to update truncation bound $b_{k,1}$ using the measurement set $Z_{b_{k,1}}$. The updates of the other three truncation bounds can be implemented similarly. In what follows, we omit the notation of iteration index t for brevity. First note that one can easily set truncation bound to $+\infty$ when its corresponding measurement set is empty. Let $f(y_1) = \mathcal{TN}(0, \Lambda_{1,1}, b_{k,1})$ and $f(r_1) = \mathcal{N}(0, R_{1,1})$ denote, respectively, the probability density function of a uni-variate truncated Gaussian distribution with density support $\{y|y > b_{k,1}\}$ and that of the Gaussian distribution with zero mean and variance $R_{1,1}$. Using the convolution formula, the density of $z_1 = y_1 + r_1$ is given by

$$f(z_1) = \frac{\Phi\left(\sqrt{\Lambda_{1,1}R_{1,1}^{-1}\zeta_{1,1}^{-1}}z_1 - \sqrt{\zeta_{1,1}\Lambda_{1,1}^{-1}R_{1,1}^{-1}}b_{k,1}\right)}{e^{0.5z_1^2\zeta_{1,1}^{-1}}\sqrt{2\pi\zeta_{1,1}}\Phi\left(-b_{k,1}\Lambda_{1,1}^{-1/2}\right)}, \quad (13)$$

where $\Phi(\cdot)$ denotes the cumulative density function of a standard Gaussian distribution, $\Lambda = \rho M_{m_k|k}^{-1} V_{k|k} (M_{m_k|k}^{-1})^T / (v_{k|k} - 6)$ is the transformed object extent matrix in the OC, and $\zeta_{1,1} = \Lambda_{1,1} + R_{1,1}$. Then, the decomposed ML estimation is to maximize the likelihood of measurement set $Z_{b_{k,1}}$ as

$$\arg \max_{b_{k,1}: b_{k,1} > 0} \prod_{z \in Z_{b_{k,1}}} f(z_1), \quad (14)$$

where z_1 is given by the x -coordinate of z . This is equivalent to minimizing the following cost function

$$\arg \min_{b_{k,1} > 0} \sum_{z \in Z_{b_{k,1}}} \left(\log \Phi(-b_{k,1}\Lambda_{1,1}^{-0.5}) - \log \Phi\left(\sqrt{\Lambda_{1,1}R_{1,1}^{-1}\zeta_{1,1}^{-1}}z_1 - \sqrt{\zeta_{1,1}\Lambda_{1,1}^{-1}R_{1,1}^{-1}}b_{k,1}\right) \right), \quad (15)$$

which can be efficiently solved with standard root-finding algorithms, e.g., Halley's method [22].

3.2.3. State Update

To integrate the hierarchical truncated Gaussian model into the random matrix-based state update [13], we make use of the converted

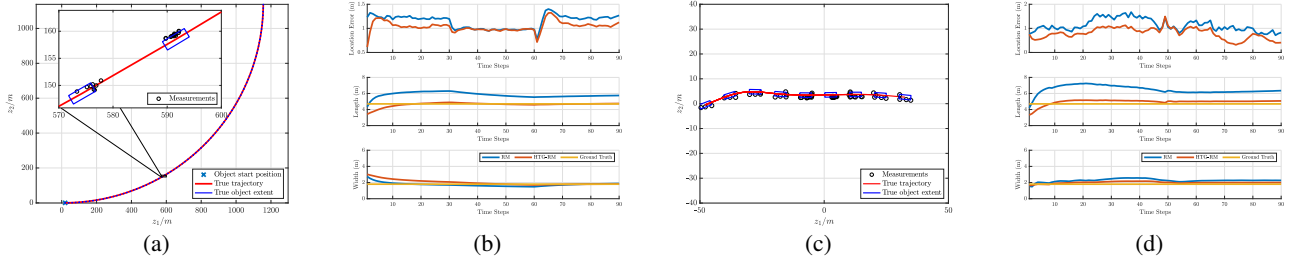


Fig. 5: Ground truth and results: (a) ground truth for scenario with synthetic measurements; (b) average estimation results over time for scenario (a); (c) ground truth for scenario with MathWorks automotive radar measurements, shown as every 10 time steps; (d) average estimation results for scenario (c).

measurement statistics by introducing pseudo measurements [20]. To achieve this, we first compute the analytical mean and spread of $n_k^c = n_k(1 - c_{D_k})/c_{D_k}$ pseudo measurements that follow a truncated Gaussian distribution with a density support $D_k^c = \mathbb{R}^2 \setminus D_k$, and then we take the weighted sum of these computed values and the sample measurement mean and spread to obtain the converted measurement mean \tilde{z}_k and spread $\Sigma_{\tilde{z}_k}$ [20].

Given the proposed measurement model (4) and the predicted density $p(\xi_k|Z_{1:k-1})$, the updated parameters $\{m, P, v, V\}_{k|k}$ determining the posterior density are given as:

$$m_{k|k} = m_{k|k-1} + K\varepsilon, \quad (16a)$$

$$P_{k|k} = P_{k|k-1} - KHP_{k|k-1}, \quad (16b)$$

$$\nu_{k|k} = \nu_{k|k-1} + (n_k + n_k^c), \quad (16c)$$

$$V_{k|k} = V_{k|k-1} + \hat{N} + \hat{Z}, \quad (16d)$$

$$\hat{N} = \hat{X}^{1/2} S^{-1/2} \varepsilon \varepsilon^T S^{-T/2} \hat{X}^{T/2}, \quad (16e)$$

$$\hat{Z} = \hat{X}^{1/2} \hat{R}^{-1/2} \Sigma_{\tilde{z}_k} \hat{R}^{-T/2} \hat{X}^{T/2}. \quad (16f)$$

where $\hat{R} = \rho \hat{X} + M_{m_{k|k}}^{(t)} R_k (M_{m_{k|k}}^{(t)})^{-1}$ and $S = HP_{k|k-1} H^T + \hat{R}/(n_k + n_k^c)$, $K = P_{k|k-1} H S^{-1}$, $\hat{X} = V_{k|k-1}/(V_{k|k-1} - 6)$ and $\varepsilon = \tilde{z}_k - Hm_{k|k-1}$.

4. SIMULATION RESULTS

In this section, we consider two scenarios in which a rectangular object (4.7-m long and 1.8-m wide) moves with a nonlinear motion for 90 time steps. We assume that the object rotation center coincides with the object physical center. The kinematic object state is defined as $x_k = [p_k, v_k, \theta_k, \omega_k]^T \in \mathbb{R}^5$ with the two-dimensional position $p_k \in \mathbb{R}^2$, polar velocity v_k , heading θ_k , and turn rate ω_k . The coordinated turn motion model is used with a sampling time of $T_s = 1s$ and standard polar and angular acceleration noise of $\sigma_{\dot{v}} = 0.1$ and $\sigma_{\dot{\omega}} = \pi/180$, respectively. The exact expressions for the transition matrix $g(\cdot)$ and process noise covariance matrix Q can be found in [23]. The transformation function E is a rotation matrix that depends on the turn rate. Given the posterior density of extent state $\mathcal{I}\mathcal{W}(X_k; \nu_{k|k}, V_{k|k})$, the estimates of length l and width w can be extracted from the normalized eigen-decomposition of the mean of the inverse Wishart distribution, $\hat{X}_k = V_{k|k}/(\nu_{k|k} - 6)$. In the implementation, the number of iterations used in the update step is set to 5 and the sliding window L has length 2.

4.1. Scenario with Synthetic Partial-View Measurements

We first consider the case that the automotive radar measurements follow the proposed measurement model over the course of the sim-

ulated trajectory, with parameters $l = 4.7$, $w = 1.8$, $\rho = 0.25$, $R_k = \text{diag}([0.125, 0.125])$, $a_{k,2} = \infty$, $b_{k,2} = 0.75$, and

$$a_{k,1} = \begin{cases} \infty, & \text{if } k \leq 60 \\ 2.14, & \text{if } k > 60 \end{cases}, \quad b_{k,1} = \begin{cases} 2.14, & \text{if } k \leq 30 \\ \infty, & \text{if } k > 30 \end{cases}.$$

The number of measurements at each time step is drawn from a Poisson distribution with mean 8. Fig. 5(a) shows two snapshots of synthesized automotive radar measurements at time step 30 and 31, respectively. It can be seen that most of these radar measurements appear to be around at most two of the object edges. We compare the tracking performance between the random matrix approach [13] (RM) and the proposed method (referred to as HTG-RM). Fig. 5(b) shows the tracking performance in terms of localization errors (w.r.t object center), and object length/width errors over time, averaged over 100 Monte Carlo runs. It can be seen from the results that the proposed HTG-RM algorithm outperforms the conventional RM approach by a large margin. Particularly, the HTG-RM algorithm provides more consistent estimates in terms of the object length and width over time.

4.2. Scenario with Independent MathWorks Measurements

To further validate the effectiveness of the proposed HTG-RM algorithm in scenarios with model mismatch, we generate the object trajectory and measurements using the MathWork Automated Driving toolbox, see Fig. 5(c) for an illustration of the ground truth. It is worth noting that the simulated measurements tend to appear around the object edge with a certain volume, which well resembles the distributional characteristics of real-world automotive radar measurements. In the implementation, the measurement model parameters are set to $R_k = \text{diag}([0.125, 0.125])$ and $\rho = 1/4$. The estimation results, averaged over 100 Monte Carlo runs, are shown in Fig. 5(d), and it can be seen that the proposed HTG-RM algorithm still outperforms the conventional RM approach [13]. Compared with the results obtained using ideal measurement model in Fig. 5(b), the HTG-RM performance is only slightly degraded, which validates the robustness of the proposed HTG-RM algorithm.

5. CONCLUSIONS

In this paper, we propose a new surface-volume measurement model for partial-view automotive radar object tracking based on a hierarchical truncated Gaussian model with adaptive truncation bounds. The proposed measurement model has been integrated into the random matrix approach by introducing pseudo measurements and online updating the truncation bounds. Our simulations validate the effectiveness of our approach.

6. REFERENCES

- [1] Karl Granström, Marcus Baum, and Stephan Reuter, "Extended object tracking: Introduction, overview, and applications," *Journal of Advances in Information Fusion*, vol. 12, no. 2, 2017.
- [2] M Buhren and Bin Yang, "Simulation of automotive radar target lists using a novel approach of object representation," in *2006 IEEE Intelligent Vehicles Symposium*. IEEE, 2006, pp. 314–319.
- [3] Joakim Gunnarsson, Lennart Svensson, Lars Danielsson, and Fredrik Bengtsson, "Tracking vehicles using radar detections," in *2007 IEEE Intelligent Vehicles Symposium*. IEEE, 2007, pp. 296–302.
- [4] Lars Hammarstrand, Malin Lundgren, and Lennart Svensson, "Adaptive radar sensor model for tracking structured extended objects," *IEEE Transactions on Aerospace and Electronic Systems*, vol. 48, no. 3, pp. 1975–1995, 2012.
- [5] Marcus Baum and Uwe D Hanebeck, "Extended object tracking with random hypersurface models," *IEEE Transactions on Aerospace and Electronic systems*, vol. 50, no. 1, pp. 149–159, 2014.
- [6] Johann Wolfgang Koch, "Bayesian approach to extended object and cluster tracking using random matrices," *IEEE Transactions on Aerospace and Electronic Systems*, vol. 44, no. 3, pp. 1042–1059, 2008.
- [7] Shishan Yang and Marcus Baum, "Tracking the orientation and axes lengths of an elliptical extended object," *IEEE Transactions on Signal Processing*, vol. 67, no. 18, pp. 4720–4729, 2019.
- [8] Peter Broßeit, Matthias Rapp, Nils Appenrodt, and Jürgen Dickmann, "Probabilistic rectangular-shape estimation for extended object tracking," in *2016 IEEE Intelligent Vehicles Symposium (IV)*. IEEE, 2016, pp. 279–285.
- [9] Xiaomeng Cao, Jian Lan, X Rong Li, and Yu Liu, "Extended object tracking using automotive radar," in *2018 21st International Conference on Information Fusion (FUSION)*. IEEE, 2018, pp. 1–5.
- [10] Niklas Wahlström and Emre Özkan, "Extended target tracking using Gaussian processes," *IEEE Transactions on Signal Processing*, vol. 63, no. 16, pp. 4165–4178, 2015.
- [11] Kolja Thormann, Marcus Baum, and Jens Honer, "Extended target tracking using Gaussian processes with high-resolution automotive radar," in *2018 21st International Conference on Information Fusion (FUSION)*. IEEE, 2018, pp. 1764–1770.
- [12] Hauke Kaulbersch, Jens Honer, and Marcus Baum, "A cartesian B-spline vehicle model for extended object tracking," in *2018 21st International Conference on Information Fusion (FUSION)*. IEEE, 2018, pp. 1–5.
- [13] Michael Feldmann, Dietrich Franken, and Wolfgang Koch, "Tracking of extended objects and group targets using random matrices," *IEEE Transactions on Signal Processing*, vol. 59, no. 4, pp. 1409–1420, 2010.
- [14] Umut Orguner, "A variational measurement update for extended target tracking with random matrices," *IEEE Transactions on Signal Processing*, vol. 60, no. 7, pp. 3827–3834, 2012.
- [15] Elif Saritaş and Umut Orguner, "A random matrix measurement update using Taylor-series approximations," in *2018 21st International Conference on Information Fusion (FUSION)*. IEEE, 2018, pp. 1–8.
- [16] Karl Granström and Umut Orguner, "A new prediction update for extended target tracking with random matrices," *IEEE Transactions on Aerospace and Electronic Systems*, vol. 50, no. 2, 2014.
- [17] Holger Caesar, Varun Bankiti, Alex H Lang, Sourabh Vora, Venice Erin Liong, Qiang Xu, Anush Krishnan, Yu Pan, Giancarlo Baldan, and Oscar Beijbom, "nuScenes: A multimodal dataset for autonomous driving," *arXiv preprint arXiv:1903.11027*, 2019.
- [18] Peter Broßeit, Bharanidhar Duraisamy, and Jürgen Dickmann, "The volcanormal density for radar-based extended target tracking," in *2017 IEEE 20th International Conference on Intelligent Transportation Systems (ITSC)*. IEEE, 2017, pp. 1–6.
- [19] Alexander Scheel and Klaus Dietmayer, "Tracking multiple vehicles using a variational radar model," *IEEE Transactions on Intelligent Transportation Systems*, 2018.
- [20] Yuxuan Xia, Pu Wang, Karl Berntorp, Toshiaki Koike-Akino, Hassan Mansour, Milutin Pajovic, Petros Boufounos, and Philip Orlik, "Extended object tracking using hierarchical truncated Gaussian measurement model," in *2020 IEEE International Conference on Acoustics, Speech and Signal Processing (ICASSP)*. IEEE, 2020.
- [21] Todd K Moon, "The Expectation-Maximization algorithm," *IEEE Signal Processing Magazine*, vol. 13, no. 6, pp. 47–60, 1996.
- [22] Walter Gander, "On Halley's iteration method," *The American Mathematical Monthly*, vol. 92, no. 2, pp. 131–134, 1985.
- [23] X Rong Li and Vesselin P Jilkov, "Survey of maneuvering target tracking. Part I. dynamic models," *IEEE Transactions on Aerospace and Electronic Systems*, vol. 39, no. 4, pp. 1333–1364, 2003.